ARTICLE

Size and Growth Rate Dependent Structural Diversification of Fe_3O_4/CdS Anisotropic Nanocrystal Heterostructures

Hunter McDaniel and Moonsub Shim*

Department of Materials Science & Engineering, University of Illinois at Urbana—Champaign, Urbana, Illinois 61801

ABSTRACT To better understand the growth mechanism leading to enhanced anisotropy in nanocrystal heterostructures synthesized from nearly spherical seeds, we have examined various factors that contribute to structural diversification in Fe_3O_4/CdS systems. Pseudoseparation of nucleation and growth allows us to quantify how the number of heterojunctions formed varies with concentration and the size of the seed nanocrystals. A careful examination of the size dependence of the maximum number of CdS particles that can nucleate per seed nanocrystal suggests strain induced limitations. By increasing the growth rate, we observe an enhancement of spatial anisotropy in rods-on-dot heterostructures without the need for rod promoting capping molecules such as phosphonic acids. Crystallographic details allow us to identify three distinct morphologies that can arise in rods-on-dot heterostructures due to zinc blende/wurtzite polytypism in CdS. In all three cases, the junction planes contain identical or nearly identical coincidence sites.

KEYWORDS: nanocrystals · heterostructures · anisotropic · iron oxide · CdS

Owing to their tunable properties and large surface-to-volume ratios, nanocrystals (NCs) are being considered for a wide range of applications including photovoltaics,[1,2] biomedical imaging,[3,4] photocatalysts,[5,6] optoelectronics,[7,8] and even rocket propellants.[9] Nanocrystal heterostructures (NCHs) are an emerging subclass of NCs where two or more chemically distinct components are brought together epitaxially.[10] The best known example is the core/shell structure where the outer shell enhances the properties of the core (e.g., increasing photoluminescence quantum yields of CdSe NCs with ZnS or CdS shell).[11−13] More recently, noncore/shell or anisotropic NCHs have been reported.[14−23] These anisotropic NCHs provide opportunities to synergistically combine unique properties of two or more materials potentially leading to entirely new ones. Before we can exploit such benefits, studies elucidating general parameters favoring anisotropic as opposed to isotropic growth are much needed. To date a few different anisotropic NCHs have been achieved and they may be categorized into two distinct types. First is the extension of nanorods or related structures where the spatial anisotropy already present in the seed material facilitates unidirectional growth of or spatially selective chemical conversion to the second component.[20−23] Second is the anisotropic nucleation from a nearly spherical seed.[14−18] One example of the latter type is Fe_3O_4/CdS NCHs where the large lattice mismatch in the presence of near coincidence site lattices[24−27] have been shown to induce anisotropic growth of the second component (i.e., in a noncore/shell manner).[14,28] Here, we examine how size and growth rate affect the overall morphology of Fe_3O_4/CdS NCHs.

The majority of the junctions formed in the anisotropic Fe_3O_4/CdS NCHs have been shown to be the near coincident {111}/{111} interface with the same zone axes when CdS is zinc blende and the equivalent {111}/{0001} interface when CdS is grown in the wurtzite structure.[14,28] Even in the presence of these coincidence site lattices, there is a small but non-negligible mismatch. Better accommodation of the residual interfacial strain in smaller NCs has been shown to allow one or a small number of CdS NCs to grow to large sizes on a small seed Fe_3O_4 NC (*i.e.*, limitations on the number of CdS nucleated), whereas starting with larger seeds easily leads to nucleation of multiple CdS NCs with limitations on the sizes achievable. To assess the possibility of single particle precision morphology engineering based on this strain effect, we first quantify the average saturation number of heterojunctions that can form on seed Fe_3O_4 NCs of varying sizes. To do so, we have separated the junction formation step from the growth step by multiple injection synthesis. This in turn allows us to vary the rate of

*Address correspondence to mshim@illinois.edu.

Received for review November 4, 2008 and accepted January 05, 2009.

Published online January 13, 2009.
10.1021/nn800737a CCC: $40.75

growth independently from heterogeneous nucleation allowing control over the average number of heterojunctions formed and providing a route to interesting rods-on-dot morphologies without the need of capping molecules that enhance unidirectional growth. Close examination of crystallographic details of the heterojunctions reveals polytypism-induced structural diversification in rods-on-dot NCHs.

RESULTS AND DISCUSSION

Separation of Junction Formation and Growth. Separation of junction formation and the ensuing CdS growth allows for a careful study of each step of the synthesis separately. Figure 1 demonstrates the technique involved for dots-on-dot morphology. Fe_3O_4 NCs are first synthesized with a narrow size distribution. A desired average number of Fe_3O_4/CdS junctions are then formed by varying the amount of Cd and S reagents added in the first injection, the "nucleation" step. Here, we refer to this first Cd/S reagent addition step as the junction formation step or nucleation step interchangeably. Subsequent Cd/S reagent addition leads to a preferential growth on the preformed nuclei. We refer to this second injection and any other additional Cd/S reagent injections as the growth steps.

To verify that the subsequent growth injections do not lead to new CdS nuclei formation, we have examined the average number of CdS NCs nucleated per seed Fe_3O_4 NC after multiple growth steps. The nucleated CdS grows larger in each growth step but even after four growth injections that were each five times the amount of CdS precursors injected for initial junction formation step, the average junction frequency remains constant as shown in Figure 2. The red shift in the absorption shoulder corresponding to CdS band edge transition further supports the increasing size of CdS due to subsequent growth injection steps (Figure S1 in Supporting Information).

Size Dependence of Saturation Number of Junctions. Having established that the junction frequency is unaltered by subsequent growth steps, we now examine how the amount of CdS precursor added in the initial nucleation step affects the junction frequency. Since the CdS "nuclei" are often difficult to distinguish, an additional growth injection consisting of 2 or 3 times the original nucleation amount of Cd/S reagents is carried out to facilitate statistical analysis. Figure 3 shows how the average number of junctions formed per seed Fe_3O_4 NC varies with the amount of CdS precursors added in the initial nucleation step for several different sizes of the seed NCs. All cases appear to have a saturation limit where the number of junctions/seed NC no longer increases with increasing amount of Cd/S reagent added. The increasing saturation number of junctions with increasing size of the seed NC is expected on the basis of previous observation that multiple CdS particle nucleation is facilitated on larger NCs.[28] The results shown in

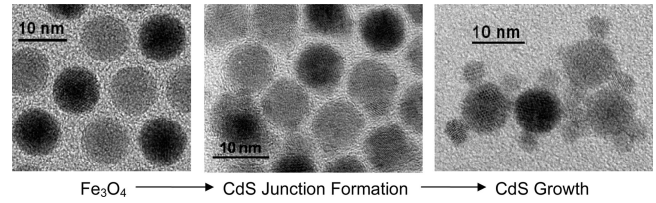

Figure 1. TEM images outlining the general synthesis procedure. In the junction formation step, Fe_3O_4 NCs appear to have small lumps which are the CdS "nuclei."

Figure 3 can now be used as "calibration curves" for synthesizing Fe_3O_4/CdS NCHs with desired average number of heterojunctions. More importantly, these results provide insights on how the saturation number of junctions scales with seed size.

To provide a more precise size dependence, 161 heterostructures have been measured from nine reactions in the junction number saturation regime (*e.g.*, at nucleation amount of 0.3 mmol for 4−5 nm size range). Figure 4A shows the seed NC diameter dependence of the

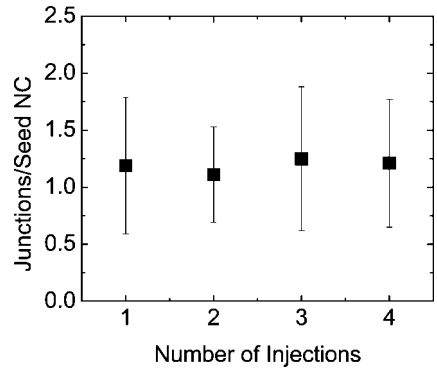

Figure 2. Average number of junctions formed per seed NC with multiple CdS growth steps (number of injections). Fe_3O_4 NCs of average diameter 6.7 nm are first nucleated with 0.1 mmol of CdS precursors. Each growth step consisted of 5× Cd/S reagent amount used for the initial nucleation. Error bars are the standard deviation of the number of junctions per seed NC counted from TEM images.

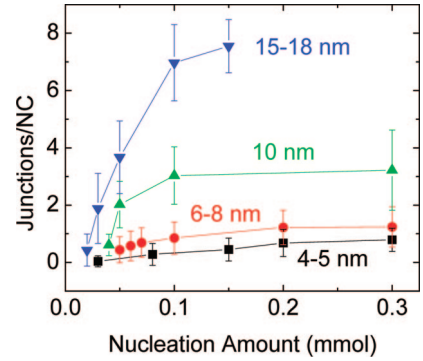

Figure 3. Dependence of the average number of heterojunctions formed per seed Fe_3O_4 NC on CdS precursor amount injected in the "nucleation" step. Each data point is a single synthesis which started with seed Fe_3O_4 in one of the four average diameter ranges as indicated. Error bars are the standard deviation of the number of junctions per seed NC counted from TEM images. Junctions/NC ≥ 7 are estimates since some of the CdS NCs may be on top or below the large Fe_3O_4 NCs and cannot be clearly distinguished.

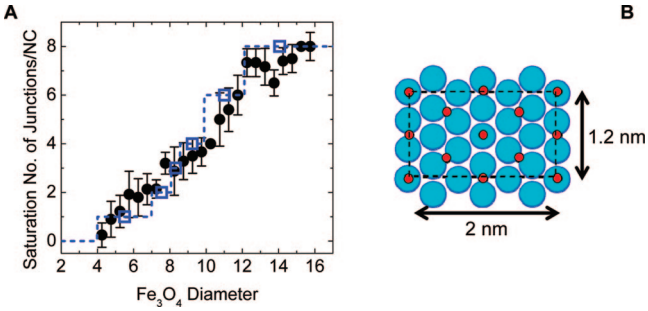

Figure 4. (A) Dependence of saturation number of junctions per NC on the seed Fe_3O_4 diameter (filled circles). Error bars are the standard deviations in the numbers counted from TEM images. Blue open squares and dashed line are expectations from a simple geometrical strain model with characteristic length of 3.5 nm as described in the text. (B) The coincidence sites on the $(111)_{Fe3O4}$ /$(111)_{CdS(Zinc\ Blende)}$ or $(0001)_{CdS(Wurtzite)}$ junction planes. Smaller red circles represent Fe atoms and the larger blue circles represent S atoms.

saturation number of CdS NCs that can nucleate per Fe_3O_4 NC. Since each reaction leads to Fe_3O_4 NCs with size distribution of about 5 to 10%, data shown are binned at diameter increments of 0.5 nm. A near linear dependence is seen in the diameter range from ~4 to ~12 nm and saturation occurs at ~8 junctions at the largest sizes indicating that the maximum number of junctions that can form on each seed particle is not a simple function of the available surface area. The initial linear behavior also suggests that this dependence on size is unlikely to be determined by the number of facets per NC which we anticipate to be independent of size for the diameter range studied here. However, the fixed number of facets per NC, especially the {111} planes of the Fe_3O_4 NCs which are always at the heterointerfaces whenever we can clearly identify the junction planes, should and does appear to place limitations on the maximum saturation number of junctions at ~8. At the small size range there is also a limitation from the surface area of the {111} planes. At ~4 nm diameter, we anticipate the {111} facets to be about 2 nm across which is about the length scale of the minimum size needed to accommodate enough coincidence sites at the heterointerface (see Figure 4B). This may then indicate the critical size for heterogeneous nucleation.

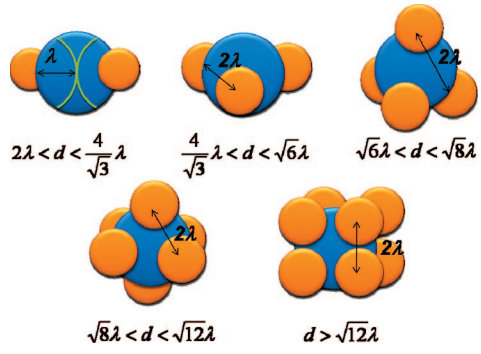

Figure 5. Schematics and the corresponding diameter range for the simple geometrical model described in the text. A fixed effective strain length (λ) leads to limitations on the maximum number of junctions per NC of a given diameter (*d*).

To account for the near linear dependence in the intermediate size regime, we consider possible effects of the strain due to an effective 2D lattice mismatch of ~4% between the coincidence planes (Figure 4B).[14,28] For simplicity, we assume that the strain field with a characteristic length λ imposes the closest possible distance between two CdS particles on the same Fe_3O_4 NC to be 2λ as schematically shown in Figure 5. We further simplify by assuming λ to be independent of size. This constraint then leads to the saturation configurations shown in Figure 5. The diameter range for each configuration comes from the following. The minimum is the diameter of the sphere in which the corresponding polyhedron of sides 2λ fits and the maximum is the diameter of the sphere in which the immediately larger size polyhedron, again with sides 2λ, fits (*e.g.*, tetrahedron and octahedron in a sphere with edges of length 2λ define the range for 4 particles on a seed NC). This simple picture would lead to steps in the diameter dependence of the saturation number of junctions at number of junctions = 1, 2, 3, 4, 6, and 8 as shown in the blue dashed line in Figure 4A. We note that if we impose the condition that only {111} facets of Fe_3O_4 can accommodate CdS growth, which is what we observe, then 3-junction case would be eliminated. However, the diameter range for 3-junction case is rather small and would not alter the dependence very much. More importantly, given that the seed NCs are likely to have variations in shape (*e.g.*, varying aspect ratios, different faceting, *etc.*), this geometrical constraint would not be strictly followed. Therefore, instead of the diameter ranges shown in Figure 5, we consider the expected saturation number of junctions with respect to the expected average diameter $\langle d \rangle$ defined as the average of the minimum and the maximum values in a given range. That is, we expect to see 2 junctions at a diameter around $(1 + 2/(3)^{1/2})\ \lambda$ and so on. The $\langle d \rangle$ value for 1 junction is set as the average of the lower limit fixed at 4 nm (based on the above argument that 4 nm is about the size at which the {111} facet area is large enough to accommodate a heterojunction) and the diameter at which the 2-junction structures begin. For the upper size limit, the $\langle d \rangle$ value for the 8 junction case is taken as the average between the minimum expected value of $(12)^{1/2}\lambda$ and the maximum experimental value of 16 nm. These geometrical expectations based on strain induced minimum distance between particles are plotted as blue open squares along with the experimental data in Figure 4A. The agreement is excellent with a reasonable value of λ = 3.5 nm. Considering variations in shape, which can only be a reduction in symmetry from simple sphere considered, would lead to less than the discrete junction frequencies of 2, 4, 6, and 8 for a given diameter (*i.e.*, the open squares in Figure 4 would shift down) but a slightly smaller value of λ, which would be closer to ~1 to 3 nm observed in TEM images, would lead to essentially the same diameter dependence.

We emphasize that this simple geometrical model serves only as an intuitive guide. One immediate correction to consider, even in the absence of shape distribution pointed out above, may be the nonuniform strain field. Following Figure 4B, every three atomic steps of S sites along either one of the directions labeled with length would lead to near coincidence with every two atomic steps for the corresponding directions in Fe sites. On the basis of lattice parameters of bulk crystals, three atomic steps of S sites are larger by ~4% than the two atomic steps for Fe. This would lead to a slight tension in the Fe_3O_4 NC in the direction parallel to the junction plane making the parallel {111} plane directly opposite to the plane on which initial CdS nucleated (as in the 2-junction case in Figure 5) better matched for second CdS to nucleate. However, other possible junction planes that are at angles between 45 and 135° to the first junction plane would become more difficult from which to nucleate (owing to positive Poisson ratio). Several additional factors including diameter-dependent strain fields, surface/interfacial relaxation,[29] interactions with capping ligands, and varying facet areas and facet-to-facet distances also need to be considered for a more complete description. All of these factors should contribute to the observed deviations from the steplike behavior expected from the simple geometrical considerations given here.

Growth Rate Dependent Heterostructure Morphology. In addition to the precursor concentration and the size dependence of the number of heterojunctions formed, the separation of junction formation step from growth allows us to examine the role of growth rate on the final NCH morphology. As a simple control over the growth rate, we have varied the amount of Cd/S reagent added in the second injection step, that is, increasing "monomer" concentration to just below the homogeneous nucleation threshold to increase growth rate. With the increased growth rate, we observe CdS rods to form on the seed Fe_3O_4 NCs. Figure 6 compares the dots-on-dot structures obtained at slow growth rates (A and C) with the rods-on-dot structures from the fast growth conditions (B and D) for two size ranges. It is interesting to note that CdS rods are grown on the seed NCs without the need for enhancing rod growth with capping molecules such as octadecyl phosphonic acid.[30,31]

Figure 7 shows how the average length and the diameter and therefore the aspect ratio of CdS evolve with the amount of reagents added in the growth step for NCHs with average seed Fe_3O_4 NC size of 7 nm. When the amount of the Cd/S reagent added for the growth step is similar to that of the initial nucleation step (i.e., at low growth rates), the resulting CdS NCs are nearly spherical as shown in TEM images of Figure 6A and C. As the ratio of Cd/S reagents added in the growth step to that added in the nucleation step increases (i.e., growth rate increases), the aspect ratio also

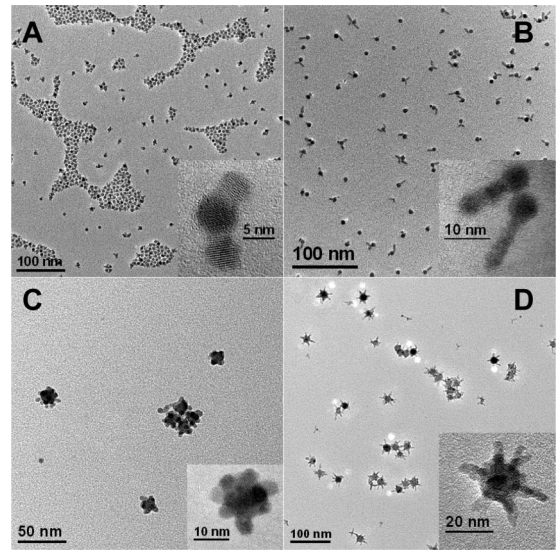

Figure 6. TEM images demonstrating rod-on-dot anisotropy dependence on precursor concentration. Smaller size seed Fe_3O_4 NCs with 1:1 (A) and 5:1 (B) growth-to-nucleation CdS precursor amount ratio leading to slow and fast CdS growth, respectively. Panels C and D are analogous to panels A and B for larger sizes of seed NCs. Higher magnification images are shown in the insets.

increases eventually leading to rods-on-dot morphologies as seen in Figure 6B and D. As expected, decreasing the overall concentration of the reaction mixture with noncoordinating solvent (while keeping the growth injection amount of Cd/S as high as when rods are achieved) leads to lower aspect ratios further confirming the effects of Cd/S reagent concentration on the growth rate and therefore the overall NCH morphology.

Wurtzite/Zinc Blende Polytypism and Structure Diversification. Previous studies on Fe_3O_4/CdS NCHs have shown that the CdS can grow as wurtzite or zinc blende.[14] This polytypism in CdS leads to diversification of possible morphologies within the rods-on-dot geometries even when the number of nuclei per seed NC can be controlled. While the structural diversity may be amplified, the rods-on-dot structures can in turn facilitate characterizing crystallographic orientations at the heterojunctions due in part to the larger sizes of the rods and in

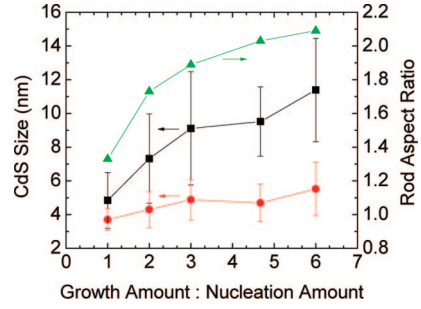

Figure 7. Evolution of average diameter (circles), length (squares), and aspect ratio (triangle) of CdS rods with increasing growth rate as represented by the ratio of amount of reagents added during the growth step to that of nucleation step. The nucleation amount consists of 0.15 mmol of CdS precursor.

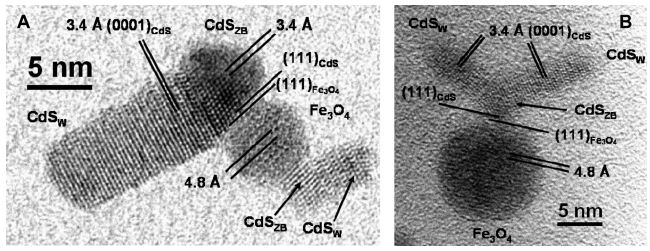

Figure 8. High resolution TEM images of branched CdS nanorods grown on Fe_3O_4 NCs. Branching occurs by initial zinc blende nucleation followed by wurtzite growth. An example is shown for small (A) and large (B) seed NCs. Note that the junction planes are the same in both cases.

part to easy-to-identify rod growth axis. There are three distinct CdS rod configurations that we have observed in the rods-on-dot NCHs. In all three configurations, CdS always grows on the {111} plane of the seed Fe_3O_4 NCs.

For NCHs with 7−9 nm Fe_3O_4 seeds, the most abundant of the three configurations is the "branched" structure (56% out of 126 junctions examined *via* high resolution TEM) as shown in Figure 8A. For the larger 15−16 nm seed diameter as shown in Figure 8B, we observe similar but slightly lower yield of these branched junctions (41% out of 79 junctions). Note that these structures sometimes have only one branch as shown in Figure 8A which then makes them appear similar to the "kinked" structures discussed later. However, the single-branch structure can be easily distinguished from the kinked structures by high resolution images showing lattice fringes and by difference in the angle of the rod growth direction with respect the Fe_3O_4 {111} plane. Branching occurs when the CdS is initially nucleated as zinc blende and fast growth conditions favoring rod

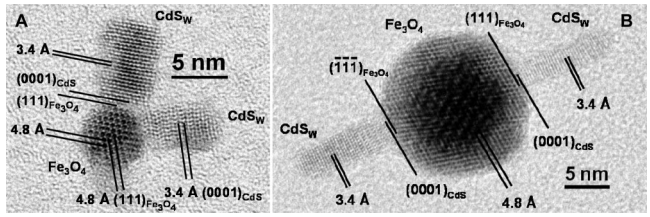

Figure 9. High resolution TEM images of linear CdS nanorods grown on Fe_3O_4 NCs. Linear rods arise from nucleation of wurtzite CdS and continued wurtzite growth. An example is shown for small (A) and large (B) seed NCs.

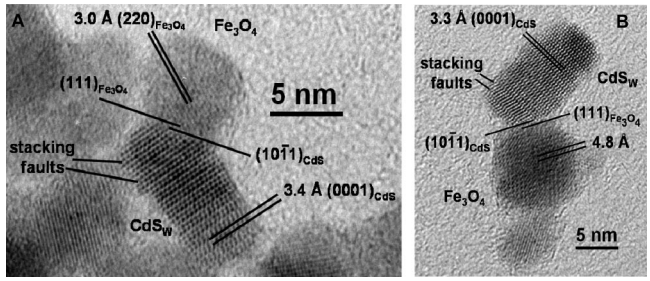

Figure 10. High resolution TEM images of kinked CdS nanorods grown on Fe_3O_4 NCs. Note the stacking fault near the junction in the CdS is often observed and may help to better accommodate the heterointerface.

growth lead to tetrapod-like structures where wurtzite rods grow out of the {111} planes of the zinc blende nuclei. The Fe_3O_4/CdS heterojunctions in these cases are the zone axes aligned {111}/{111} planes with coincidence sites shown in Figure 4B.

For the smaller 7−9 nm seed size range, the second most abundant configuration observed is the linear structure (27%) as shown in Figure 9A. At the larger seed size of 15−16 nm, we observe a substantial increase in the yield of these junctions (58%) as shown in Figure 9B. These linear structures arise from CdS being nucleated as wurtzite and continuing to grow in the same crystal structure with preferential growth along the <0001> direction. The heterointerfaces in this configuration are the same junction planes with coincidence sites as shown in Figure 4B with the {0001} planes for CdS which is equivalent to the {111} planes of zinc blende.

The less frequently observed NCH morphology is shown in Figure 10. This "kinked" structure, which is observed ~15% of the time for the smaller 7−9 nm seed NCs and only ~1% of the times for the larger 15−16 nm seeds, arises from wurtzite CdS growth. The heterojunction in this case consists of {111}/{10$\bar{1}$1} interface. A schematic of this interface is show in Figure S2 of the Supporting Information. These kinked structures are also often associated with stacking faults near the Fe_3O_4/CdS interface as indicated in Figure 10. The {10$\bar{1}$1} plane of wurtzite is a near close-packed plane, that is, similar to the {0001} plane. Incorporating the stacking faults, the CdS part of the interface then becomes the same as or very close to the junction plane with coincidence sites shown in Figure 4B. We believe that the main reason for the low yields of these kinked structures on larger seed Fe_3O_4 NCs may be associated with interfacial strain. The smaller seed NCs will likely accommodate strain better making it more versatile for the CdS {10$\bar{1}$1} junction plane to form.

CONCLUSION

We have shown that the junction formation step can be separated from growth while the average number of CdS particles growing on Fe_3O_4 can be maintained in anisotropic NCH synthesis. By doing so, we have been able to examine how the maximum number of heterojunctions that can form depend on the size of the seed NCs and how the growth rate affects the resulting NCH morphology. The emerging picture of the growth mechanism for anisotropic Fe_3O_4/CdS NCHs from the results obtained is as follows. CdS can nucleate on {111} planes of seed Fe_3O_4 NCs in either wurtzite or zinc blende form. Slow growth leads to dots-on-dot morphologies where the maximum number of CdS that can grow on Fe_3O_4 is mainly determined by the interfacial strain. The strain may be considered to limit the nearest possible distance between growing CdS particles. Rods-on-dot structures arise at fast growth

rates and these structures provide insights on the heterointerfaces and how polytypism in CdS leads to three distinct morphologies: "branched" structure when CdS nucleates as zinc blends and "linear" and "kinked" structures with wurtzite nucleation. The branched and the linear structures have the same junction planes with coincidence sites, that is, $\{111\}_{CdS(Zinc\ Blende)}$ or $\{0001\}_{CdS(Wurtzite)}$ aligned with $\{111\}_{Fe3O4}$. The CdS junction planes of kinked structures are $\{10\bar{1}1\}$ planes which in the presence of stacking faults may become nearly identical to the {0001} planes at the interface. While the overall wurtzite to zinc blende ratio of the CdS nuclei does not appear to change very much with size, the linear-to-kinked ratio increases with increasing seed Fe_3O_4 size which may also be attributed to strain effects.

METHODS

All syntheses were carried out using standard airless techniques under N_2. Reagents were used as received. All steps of the synthesis described below were carried out as a one-pot synthesis where the reaction mixture is always kept in the same reaction vessel under N_2. Small aliquots were taken out of the reaction mixture after each step for characterization.

Synthesis of Fe_3O_4 NCs. Fe_3O_4 NCs were prepared in a 50 mL three neck round-bottom flask with a reflux condenser by thermal decomposition of 0.2 mL of $Fe(CO)_5$ in a vacuum degassed solvent of dioctyl ether and oleic acid according to ref 32. The average size of the NCs was controlled by changing the amounts of oleic acid and dioctyl ether, while the amount of iron pentacarbonyl was kept constant in all syntheses. As an example, 10 mL of dioctyl ether and 1.1 mL of oleic acid were used to make NCs with 7 nm average diameter. We note that vacuum degassing of the solvent to consistent dryness is important in achieving desired size of Fe_3O_4 with narrow size distribution.

Heterojunction Formation. Following the synthesis of Fe_3O_4 NCs, the reaction mixture was cooled to 100 °C under N_2 and an indicated amount of 1 M bis-trimethylsilylsulfide (TMS_2S) in 3 mL of trioctylphosphine (TOP) was injected. The solution was then heated up to 180 °C at ~15 °C/min and held at this temperature for 5 min before cooling to 60 °C. An equimolar amount (1:1 Cd:S) of 1 M $Cd(CH_3)_2$ in TOP was then added dropwise to the reaction mixture. After 5 min of vigorous stirring the solution was heated at ~15 °C/min to 250 °C and maintained at this temperature for 30 min. The amount of CdS precursors injected for this junction formation step determined the average frequency of heterojunctions formed per seed NC.

Subsequent growth of CdS. Following the nucleation step, the reaction mixture was cooled to 60 °C and indicated amounts of 0.5 M $Cd(CH_3)_2$ and TMS_2S in TOP (1:1 Cd:S molar ratio) were added dropwise. After stirring for 5 min, the solution was heated up to 200 °C at ~15 °C/min and annealed for 1 h. At annealing temperatures of 200 °C and below, the rods-on-dot geometry is maintained but higher temperature annealing (*e.g.*, reflux at ~280 °C) causes structures to slowly revert to dots-on-dot morphologies. The resulting NCHs can be precipitated with ethanol and redissolved in nonpolar solvents. The molar ratio of growth injection of CdS precursors to the nucleation amount determines the aspect ratio of the epitaxially grown CdS. Smaller growth/nucleation Cd/S reagent ratios lead to spherical CdS grown on Fe_3O_4 NCs while higher ratios lead to CdS rod growth. Injecting more than 6× the amount of Cd/S reagent for the growth step than the nucleation step generally leads to homogeneous nucleation of isolated CdS NCs. This is independent of the nucleation amount. Adding oleic acid before the growth step greatly reduced the aspect ratio for CdS. The overall junction formation and growth of CdS on Fe_3O_4 NCs are outlined in the series of TEM images in Figure 1.

Characterization of NCHs. Transmission electron microscopy (TEM) samples were prepared using a dilute chloroform solution of NCs on Cu grids coated with a thin carbon film (Tedpella Inc.). TEM analysis was conducted with a JEOL 2010 LaB6 operating at 200 kV. Powder X-ray diffraction (PXRD) measurements were carried out on a Rigaku Geigerflex with a D-MAX system. Fe_3O_4 NCs typically had a standard size deviation of 6%. Samples with higher than 10% size distribution were not included in the statistical analysis. In all plots shown, the error bars are the standard deviation in the TEM statistics from the average value which is the plotted point.

Acknowledgment. This material is based upon work supported by ACS PRF under Grant No. 46443-AC10 and by the Nanoscale Science and Engineering Initiative of the National Science Foundation under NSF Award Number DMR-0642573. Transmission electron microscopy was carried out in the Center for Microanalysis of Materials, University of Illinois at Urbana−Champaign, which is partially supported by the U.S. Department of Energy under Grant No. DEFG02-91-ER45439.

Supporting Information Available: Absorption spectra of Fe_3O_4/CdS nanocrystal heterostructures at each CdS growth step and a schematic of the $\{111\}/\{10\bar{1}1\}$ heterointerface. This material is available free of charge *via* the Internet at http://pubs.acs.org.

REFERENCES AND NOTES

1. Kamat, P. V. Meeting the Clean Energy Demand: Nanostructure Architectures for Solar Energy Conversion. *J. Phys. Chem. C* **2007**, *111*, 2834–2860.
2. Gur, I.; Fromer, N. A.; Geier, M. L.; Alivisatos, A. P. Air-Stable All-Inorganic Nanocrystal Solar Cells Processed From Solution. *Science* **2005**, *310*, 462–465.
3. Medintz, I. L.; Uyeda, H. T.; Goldman, E. R.; Mattoussi, H. Quantum Dot Bioconjugates for Imaging, Labelling, and Sensing. *Nat. Mater.* **2005**, *4*, 435–446.
4. Michalet, X.; Pinaud, F. F.; Bentolila, L. A.; Tsay, J. M.; Doose, S.; Li, J. J.; Sundaresan, G.; Wu, A. M.; Gambhir, S. S.; Weiss, S. Quantum Dots for Live Cells, *in Vivo* Imaging, and Diagnostics. *Science* **2005**, *307*, 538–544.
5. Chen, X.; Mao, S. S. Titanium Dioxide Nanomaterials: Synthesis, Properties, Modifications, and Applications. *Chem. Rev.* **2007**, *107*, 2891–2959.
6. Wang, C. J.; Kwon, K. W.; Odlyzko, M. L.; Lee, B. H.; Shim, M. PbSe Nanocrystal/TiO*x* Heterostructured Films: A Simple Route to Nanoscale Heterointerfaces and Photocatalysis. *J. Phys. Chem. C* **2007**, *111*, 11734–11741.
7. Caruge, J. M.; Halpert, J. E.; Wood, V.; Bulovic, V.; Bawendi, M. G. Colloidal Quantum-Dot Light-Emitting Diodes With Metal-Oxide Charge Transport Layers. *Nat. Photon.* **2008**, *2*, 247–250.
8. Zhao, J. L.; Bardecker, J. A.; Munro, A. M.; Liu, M. S.; Niu, Y. H.; Ding, I. K.; Luo, J. D.; Chen, B. Q.; Jen, A. K. Y.; Ginger, D. S. Efficient CdSe/CdS Quantum Dot Light-Emitting Diodes Using a Thermally Polymerized Hole Transport Layer. *Nano Lett.* **2006**, *6*, 463–467.
9. Armstrong, R. W.; Baschung, B.; Booth, D. W.; Samirant, M. Enhanced Propellant Combustion with Nanoparticles. *Nano Lett.* **2003**, *3*, 253–255.
10. Cozzoli, P. D.; Pellegrino, T.; Manna, L. Synthesis, Properties, and Perspectives of Hybrid Nanocrystal Structures. *Chem. Soc. Rev.* **2006**, *35*, 1195–1208.
11. Hines, M. A.; Guyot-Sionnest, P. Synthesis and Characterization of Strongly Luminescing ZnS-Capped CdSe Nanocrystals. *J. Phys. Chem.* **1996**, *100*, 468–471.
12. Dabbousi, B. O.; RodriguezViejo, J.; Mikulec, F. V.; Heine, J. R.; Mattoussi, H.; Ober, R.; Jensen, K. F.; Bawendi, M. G.

(CdSe)ZnS Core-Shell Quantum Dots: Synthesis and Characterization of a Size Series of Highly Luminescent Nanocrystallites. *J. Phys. Chem. B* **1997**, *101*, 9463–9475.
13. Peng, X. G.; Schlamp, M. C.; Kadavanich, A. V.; Alivisatos, A. P. Epitaxial Growth of Highly Luminescent CdSe/CdS Core/Shell Nanocrystals with Photostability and Electronic Accessibility. *J. Am. Chem. Soc.* **1997**, *119*, 7019–7029.
14. Kwon, K. W.; Shim, M. γ-Fe_2O_3/II-VI Sulfide Nanocrystal Heterojunctions. *J. Am. Chem. Soc.* **2005**, *127*, 10269–10275.
15. Figuerola, A.; Fiore, A.; Di Corato, R.; Falqui, A.; Giannini, C.; Micotti, E.; Lascialfari, A.; Corti, M.; Cingolani, R.; Pellegrino, T.; Cozzoli, P. D.; Manna, L. One-Pot Synthesis and Characterization of Size-Controlled Bimagnetic FePt-Iron Oxide Heterodimer Nanocrystals. *J. Am. Chem. Soc.* **2008**, *130*, 1477–1487.
16. Gao, J. H.; Zhang, B.; Gao, Y.; Pan, Y.; Zhang, X. X.; Xu, B. Fluorescent Magnetic Nanocrystals By Sequential Addition of Reagents in a One-Pot Reaction: A Simple Preparation for Multifunctional Nanostructures. *J. Am. Chem. Soc.* **2007**, *129*, 11928–11935.
17. Xu, C.; Xie, J.; Ho, D.; Wang, C.; Kohler, N.; Walsh, E. G.; Morgan, J. R.; Chin, Y. E.; Sun, S. Au-Fe_3O_4 Dumbbell Nanoparticles as Dual-Functional Probes. *Angew. Chem., Int. Ed.* **2008**, *47*, 173–176.
18. Choi, S. H.; Kim, E. G.; Hyeon, T. One-Pot Synthesis of Copper-Indium Sulfide Nanocrystal Heterostructures with Acorn, Bottle, and Larva Shapes. *J. Am. Chem. Soc.* **2006**, *128*, 2520–2521.
19. Talapin, D. V.; Yu, H.; Shevchenko, E. V.; Lobo, A.; Murray, C. B. Synthesis of Colloidal PbSe/PbS Core-Shell Nanowires and PbS/Au Nanowire-Nanocrystal Heterostructures. *J. Phys. Chem. C* **2007**, *111*, 14049–14054.
20. Mokari, T.; Sztrum, C. G.; Salant, A.; Rabani, E.; Banin, U. Formation of Asymmetric One-Sided Metal-Tipped Semiconductor Nanocrystal Dots and Rods. *Nat. Mater.* **2005**, *4*, 855–863.
21. Koo, B.; Korgel, B. A. Coalescence and Interface Diffusion in Linear CdTe/CdSe/CdTe Heterojunction Nanorods. *Nano Lett.* **2008**, *8*, 2490–2496.
22. Kumar, S.; Jones, M.; Lo, S. S.; Scholes, G. D. Nanorod Heterostructures Showing Photoinduced Charge Separation. *Small* **2007**, *3*, 1633–1639.
23. Demchenko, D. O.; Robinson, R. D.; Sadtler, B.; Erclonmez, C. K.; Alivisatos, A. P.; Wang, L. W. Formation Mechanism and Properties of CdS-Ag_2S Nanorod Superlattices. *ACS Nano* **2008**, *2*, 627–636.
24. Bollmann, W. *Crystal Defects and Crystalline Interfaces*; Springer-Verlag: Berlin, 1970.
25. Brokman, A.; Balluffi, R. W. Coincidence Lattice Model for the Structure and Energy of Grain Boundaries. *Acta Metall.* **1981**, *29*, 1703–1719.
26. Trampert, A.; Ploog, K. H. Heteroepitaxy of Large-Misfit Systems: Role of Coincidence Lattice. *Cryst. Res. Technol.* **2000**, *35*, 793–806.
27. Li, B. Q.; Zuo, J.-M. The Development of Epitaxy of Nanoclusters on Lattice-Mismatched Substrates: Ag on H−Si(111) Surfaces. *Surf. Sci.* **2002**, *520*, 7–17.
28. Kwon, K. W.; Lee, B. H.; Shim, M. Structural Evolution in Metal Oxide/Semiconductor Colloidal Nanocrystal Heterostructures. *Chem. Mater.* **2006**, *18*, 6357–6363.
29. Leung, K.; Whaley, K. B. Surface Relaxation in CdSe Nanocrystals. *J. Chem. Phys.* **1999**, *110*, 11012–11022.
30. Yin, Y.; Alivisatos, A. P. Colloidal Nanocrystal Synthesis and the Organic−Inorganic Interface. *Nature* **2005**, *437*, 664–670.
31. Manna, L.; Milliron, D. J.; Meisel, A.; Scher, E. C.; Alivisatos, A. P. Controlled Growth of Tetrapod-Branched Inorganic Nanocrystals. *Nat. Mater.* **2003**, *2*, 382–385.
32. Hyeon, T.; Lee, S. S.; Park, J.; Chung, Y.; Na, H. B. Synthesis of Highly Crystalline and Monodisperse Maghemite Nanocrystallites without a Size-Selection Process. *J. Am. Chem. Soc.* **2001**, *123*, 12798–12801.